ACS APPLIED BIO MATERIALS

www.acsabm.org Article

Nanometer-Thick Superhydrophobic Coating Renders Cloth Mask Potentially Effective against Aerosol-Driven Infections

Prerona Gogoi, Sunil Kumar Singh, Ankur Pandey, Arun Chattopadhyay,* and Partho Sarathi Gooh Pattader*

Cite This: https://doi.org/10.1021/acsabm.1c00851 Read Online

ACCESS | Metrics & More | Article Recommendations | Supporting Information

ABSTRACT: The advent of COVID-19 pandemic has made it necessary to wear masks across populations. While the N95 mask offers great performance against airborne infections, its multilayered sealed design makes it difficult to breathe for a longer duration of use. The option of using highly breathable cloth or silk masks especially for a large populace is fraught with the danger of infection. As a normal cloth or silk mask absorbs airborne liquid, it can be a source of plausible infection. We demonstrate the chemical modification of one such mask, Eri silk, to make it hydrophobic (contact angle of water is 143.7°), which reduces the liquid absorption capacity without reducing the breathability of the mask significantly. The breathability reduces only 22% for hydrophobic Eri silk compared to the pristine Eri silk, whereas N95 shows a 59% reduction of breathability. The modified hydrophobic silk can repel the incoming aqueous liquid droplets without wetting the surface. The results indicate that a multilayered modified silk mask to make it hydrophobic can be an affordable and breathable alternative to the N95 mask.

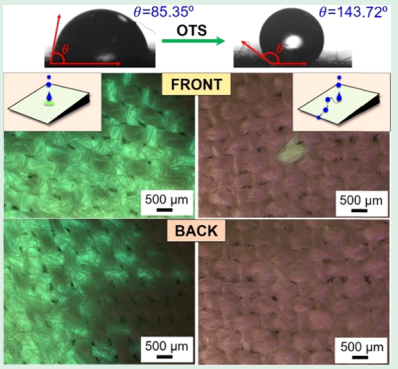

KEYWORDS: *masks, SARS-CoV-2, superhydrophobic, octadecyltrichlorosilane, aerosol-driven infections*

1. INTRODUCTION

The ubiquitous presence of facemask globally in the context of the ongoing coronavirus disease-2019 (COVID-19) pandemic underscores the need for effective preparations for prevention against aerosol-driven infections. It has been proven beyond doubt that wearing a facemask is an effective way of preventing rapid transmission of infection due to severe acute respiratory syndrome coronavirus-2 (SARS-CoV-2) through airborne droplets, especially when treatment options are still evolving. For example, although the risk of infection of SARS-CoV-2 is high within 1 m of separation,[1] studies indicate that the transmission can be prevented in a community through the use of masks.[2] It is also important to emphasize that universal access to high-performance masks is arguably one of the easiest ways of ensuring healthcare for a large populace.

The World Health Organization (WHO) recommends wearing N95 masks as a protective measure from infection due to SARS-CoV-2,[3] which has an efficiency of 95% or more to block 0.3 μm particles.[4] An N95 mask is usually made up of four layers: first is a polymeric hydrophobic microfiber[5] layer to repel droplets, second is a support layer that provides rigidity, the third layer is the nonwoven meltblown polypropylene, and the fourth is again a hydrophobic layer that prevents internally created moistures from entering the filter.[6] Commercially available surgical masks are usually three-layered with a hydrophobic outer layer,[7,8] and the middle polypropylene[9] layer usually has the smallest fiber of 5.7 ± 2.8 μm diameter to act as a filtration medium.[10] Surgical masks have a filtration efficiency of >80% with respect to 50−500 nm particles; however, a significant amount of particles within the 100 nm range can easily pass through them.[6] Surgical and N95 masks act as better protectors against the aerosol-driven virus but are expensive and thus are mostly used by medical personnel, scientist, and other working professionals. On the other hand, there is also demand for cost-effective and easily available alternatives, especially cloth and silk masks that suffice to meet the American Society for Testing and Materials (ASTM) standards.[11−13] However, it is reported that the transmission probability of aerosol particles through cloth mask is greater than N95.[14] The filtration efficiency of cloth mask depends on factors such as fabric type, width, yarn count, and mass. Some silk fabrics are hydrophilic, such as the Eri silk[15] and Paat silk,[13] and some are hydrophobic, such as Muga silk.[16] Masks made of cotton, natural silk, or chiffon with tighter weave are 50% effective, and four-layered silk is >85% effective in blocking droplets of size range 10 nm to 6 μm.[17] In addition to that, 600 TPI cotton provides excellent efficiency of 98% by blocking 300 nm to 6 μm aerosol droplets.

Received: August 1, 2021
Accepted: September 30, 2021

In addition to the nature of the mask, factors such as exhale-to-inhale (E:I) ratio, the gap between the mask and the nose may affect the efficiency of different types of layered masks.[18] Following sneezing, the droplets can travel distances ranging from 0.5 to 0.8 m in the forward direction for a layered or surgical mask.[19] However, the sneezing droplets leaked from the sides and top of the N95 mask due to gaps between the nose and the mask can remain suspended in the air and travel 0.6 m backward. It is also reported that the secondary atomization of the droplets while passing through the different layers of masks[20] is also an important factor to be considered during selecting a mask along with appropriate filter materials and the number of layers. A double-layered surgical mask can block about 92% of the initial cough droplets of size 620 μm, whereas the secondary atomized droplets (diameter <100 μm) consist of about 28% total droplets transmitted[20] possessing a greater risk of transmitting the disease. Moreover, the range of droplet transmission fraction is from 0.1% in the N95 mask to 110% for polyester/spandex neck gaiter, which is higher if not wearing a mask is considered as 100%.[21]

Although the N95 mask is designed to provide 95% protection against airborne viruses, the reported penetration value for virions of 10−80 nm is 5.6% at a relatively high flow rate of 85 L/min in the certification test.[22] Also, a recent report suggests that the infection from a pathogen-laden filter needs to be considered seriously as SARS-CoV-2 can become airborne from the same.[23] A strong flow of air induced by inhalation through the contaminated filter may worsen the situation, especially when wearing a mask for the whole day.

However, fundamental to the workings of the masks is the materials and designs used to fabricate the same. For example, in a multilayered N95 mask, the major filtration work is done by the 100−1000 μm thick meltblown hydrophobic[24,25] polypropylene fiber layer.[26] A comfortable mask should have a pressure drop <8 mm water column (WC),[27] but N95 specifications make a higher pressure drop of 25−35 mm WC[6,27] and even encounter breathing resistance of 142−1 Pa.[28] As cloth or silk masks are flexible and comfortable to wear with less suffocation compared to N95,[27,28] chemical modification of such mask materials is a potential strategy to improve their performance. For example, copper (Cu)/silver (Ag) nanoparticle-incorporated reduced graphene oxide (RGO) coating increases the efficiency of cotton as a protective measure.[29] Additionally, charged[30,31] polystyrene fiber with electret effect[32] provided a high filtration efficiency of about 99.8% with a low air resistance of only 72 Pa, making it a suitable material for manufacturing a mask.[33] While large droplets (>1 μm) settle due to gravitational force after being exhaled[17,24] or adhere to the mask fibers due to the inertial impaction,[34,35] the smaller droplets (<1 μm) may float around for a considerable time and diffuse through the pores of filters due to Brownian motion or adhere to the fiber due to interception.[34,36] Thus, to understand the transfer routes of pathogens to the human body, it is important to probe interactions between aerosol droplets and the fiber of the mask materials.

A thin and rather porous cloth mask is expected to provide the least protection against aerosol-driven viral infection. This is due to the rapid absorption of water droplets by the hydrophilic[37] cotton or silk fabrics within 7 s.[38] Hence, the question remains whether the chemical modification of the hydrophilic cotton or silk masks to hydrophobic masks retains the comfortability of breathing and at the same time provides better protection against viral infection. Herein, we report that nanometer-thick coatings by superhydrophobic molecule octadecyltricholorosilane (OTS) rendered cotton and silk fabrics resistant to the passing of aerosol droplets and thus potential mask materials against aerosol-driven viral disease such as COVID-19. Further, with high oxygen permeability, even after coating with the superhydrophobic molecule compared to the N95 mask, they provide superior options for ease of breathing with a high level of protection against aerosol-borne viral diseases such as SARS-CoV-2 for a large populace.

2. RESULTS AND DISCUSSION

2.1. Hydrophobicity and Liquid Absorption Capacity of Mask Fabrics. Our central aim has been to study the behavior of different types of masks when sprayed from a distance with model aerosol. The types of masks and their nomenclature used in this work are presented in Table 1.

Table 1. Types of Masks Used in the Current Study[a]

nomenclature	type of mask	layers present	characteristic of mask
A	Cloth 1	2 layers/3 layers	hydrophilic[7]
B	Cloth 2	2 layers/3 layers	hydrophobic
C	Muga silk	2 layers/3 layers	hydrophobic[16]
D	Eri silk	2 layers/3 layers	hydrophilic[15]
E	Paat silk	2 layers/3 layers	hydrophilic[13]
F	surgical	3 layers	hydrophobic[8]
G	N95	5-layer filtration membrane technology	hydrophobic[5]
	superhydrophobic	??	

[a]The Superscripts in the Last Column Denote References.

A first impression about the effectiveness of a mask against an incoming aerosol can be made from the fractional area coverage on the outer layer of the mask upon impact. We pursued this by placing the mask cloth sample (4 cm × 4 cm) at one end of an enclosed chamber, 30 cm away from the other end having an opening for a spray bottle that sprayed aerosol (Figure 1a). The chamber was maintained at 23 ± 2 °C and a relative humidity of ∼58 ± 2%. The liquid used was a fluorescein salt solution in 60% (v/v) aqueous glycerol. The air-dried fabric was viewed under a fluorescence microscope and then the fractional area coverage of the deposited dye was calculated using the open-source software ImageJ. A plot of correlation between the fractional coverage of the absorbed dye with the hydrophobicity of the mask fabric is shown in Figure 1b. The hydrophobicity of the mask fabric was measured based on the contact angle of water on the fabric. It was observed that the hydrophobic mask fabric (with a higher water contact angle) had lower fractional coverage of the dye in comparison to hydrophilic mask fabric (having a lower contact angle). For example, the water contact angle for N95 mask fabric (sample G) was ∼127.4° ± 3.39 and the fractional coverage for the same was ∼6% ± 0.028. On the other hand, the cotton cloth 1 sample (sample A) with a water contact angle of ∼66.7° ± 3.71 had a fractional coverage of ∼56% ± 0.098. As is clear from Figure 1b, the water contact angles and fractional dye coverage for all other mask fabrics were measured to have values in between the above ranges (as applicable) (see Supporting Information Table S1). Impor-

https://doi.org/10.1021/acsabm.1c00851
ACS Appl. Bio Mater. XXXX, XXX, XXX−XXX

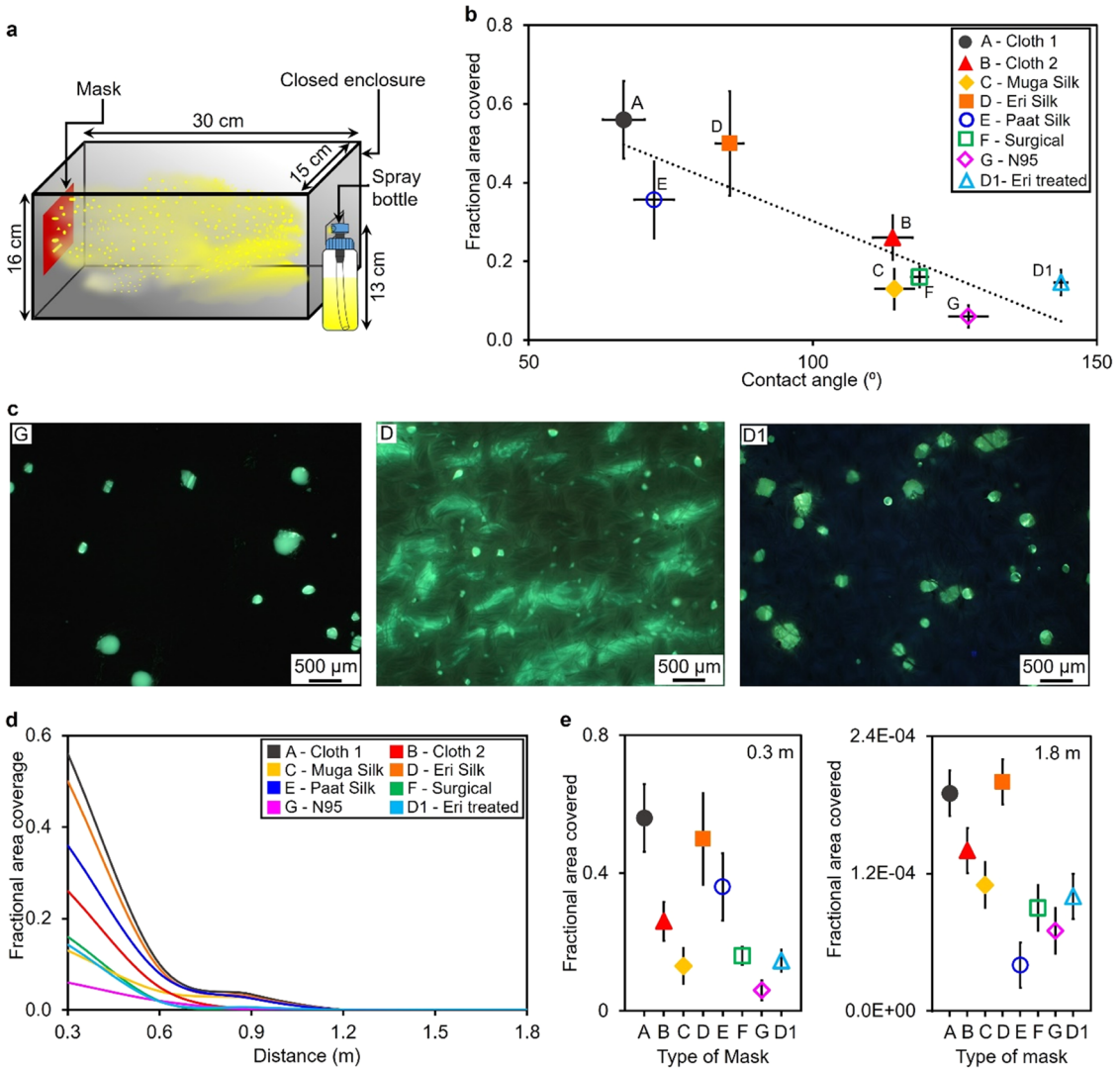

Figure 1. Fractional area covered on masks. (a) Schematic showing the experimental setup of a cuboidal enclosure of length ~30 cm that had a mask on one end and an opening for spraying from the other end. (b) Graph depicting the fractional area coverage of the absorbed dye after drying of the deposited droplets as a function of the contact angle of water on the mask materials. The black dotted line is the linearly fitted curve. (c) Typical fluorescence micrograph of the mask sample after spraying of two puffs from a spray bottle kept 30 cm away in an enclosure shown in the experimental setup; D: Eri Silk, G: N95, D1: Treated Eri silk. Additional trial images are provided in Supporting Information Figure S4. (d) Graph showing the fractional area covered for different types of masks at different distances ranging from 0.3 to 1.8 m. (e) Comparative graphs showing the sharp decline in fractional area coverage at distances 0.3 and 1.8 m, respectively. Corresponding data are provided in Supporting Information Table S3.

tantly, the as-purchased Eri silk fabric had a water contact angle of 85.4° ± 2.4 and also had a high dye fractional coverage area of 50% ± 0.133. The OTS-treated Eri silk, on the other hand, exhibited excellent hydrophobic properties with a water contact angle of 143.7° ± 1.13 and fractional area coverage of only 14.6% ± 0.032, which is better than most of the masks reported here (Table S1 in the Supporting Information). Fluorescence microscopy images for the area coverage of absorbed dye after drying on different types of masks are shown in Figure S4 of the Supporting Information. The OTS-treated cotton cloth 1 (sample A) also displayed hydrophobic characteristics with a water contact angle of 140.4° (see Supporting Information Figure S5). Similarly, fluorescence microscopy images (Figure 1c) of samples G, D, and D1 also showed that the area covered by the sprayed droplets on sample G is the least followed by D1 and D. The results clearly indicated that by modifying the hydrophobicity of mask material or fabric, it was possible to have superior performance against aerosol. Thus, an affordable mask can be chemically tailored to have better protection against viral infection that spreads through aerosol.

An important parameter that determines the plausibility of viral infection is the physical distance of separation of the recipient from the source. In other words, it is important to understand the profiles of the impression of aerosol droplets that contain a chosen molecule (as a model for pathogen) on the mask fabric as a function of the distance of separation from the source. To emulate the profile, we fabricated a cylindrical tunnel, with a spray bottle at one end (source of droplets) and a test mask sample fabric fitted at a particular distance (0.3–1.8 m) from the source. The fractional area coverage versus distance for all of the samples are plotted in Figure 1d (and is also presented in Supporting Information Table S2). Further, as is clear from the figure, the fractional area coverage

https://doi.org/10.1021/acsabm.1c00851
ACS Appl. Bio Mater. XXXX, XXX, XXX−XXX

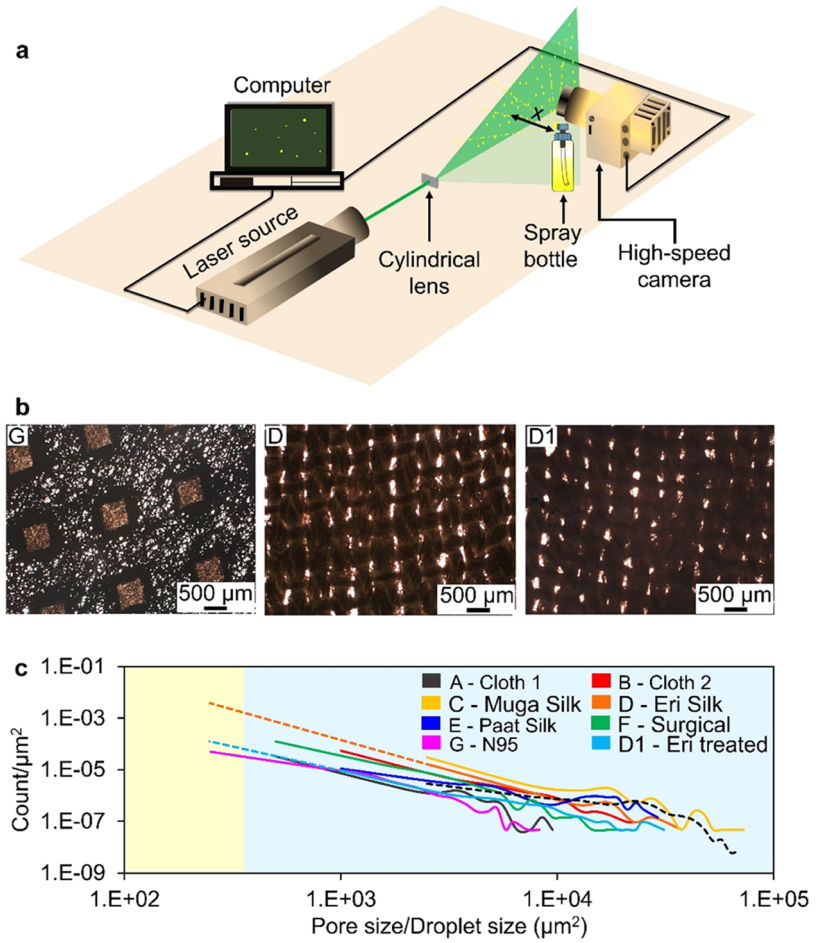

Figure 2. (a) Experimental setup showing the method used for measuring the droplet size spread after spraying from a bottle. A laser sheet is used to illuminate the droplets, and the image was recorded with a high-speed camera (Phantom VEO 640L) at 300 fps. Here, "*x*" is the distance between the spray nozzle and the laser sheet. The values of *x* were 5, 10, and 15 cm. (b) Transmission optical micrograph of the pore sizes of the first layer of the mask materials: the sample names (G, D, D1) indicated in the images correspond to those mentioned in Table 1. Additional images of other masks and the corresponding FESEM images are provided in Supporting Information Figures S6 and S7, respectively. (c) Graph showing the pore size distribution of all types of masks. The black dotted line is the droplet size distribution plot for the value of x = 10 cm. Similar data with droplet size distribution for the value of x = 5 and 15 cm are presented in Supporting Information Figure S8.

decreased quickly from a distance of 0.3−0.6 m for all of the fabrics. At 0.3 m of distance, the fractional coverage (Figure 1d) was high for Cloth 1 (56%) and Eri silk (50%) fabrics; whereas it was moderate for Paat silk (36%) and Cloth 2 (26%). On the other hand, the coverage was low for OTS-treated Eri silk (14.6%), muga silk (13%), surgical mask (16%), and N95 mask (6%). The results indicated that the more hydrophobic the fabric was, the less fractional area coverage for the deposited dye was at 0.3 m. Importantly, as shown in Figure 1e, at 1.8 m, the fractional area coverage for all samples was reduced by 99.9% with respect to the fractional area coverage at 0.3 m. Moreover, trends in coverage were similar for both at 0.3 and 1.8 m. In view of the above, we subsequently focused on characteristics at a 0.3 m distance between the source and the sample mask fabric.

2.2. Droplet Size and Porosity of Mask. To estimate the droplet size distribution at a particular distance, an experimental setup consisting of a high-speed camera (Phantom VEO 640L, 512 ×512 resolution, 300 fps), which can capture the droplets illuminated with a laser sheet, was used (Figure 2a). The droplets were sprayed from a bottle placed at different distances from the laser sheet. A laser beam that came out of a laser source (RayPower 450, Dantec Dynamics) was converted to a laser sheet with the help of a cylindrical lens. The droplet images thus captured were then analyzed with an open-source software ImageJ, and the distribution of the droplet size was constructed from 3000 data points extracted from three individual files of the recorded images using Origin software.

The microscopic images in the transmittance mode revealed that the materials for the cloth masks (samples A, B) and the silk masks (samples C, D, E) (Figures 2b and S6) have been interwoven to form rectangular pore arrangements of different sizes. Sample C has the largest pore size of around 72 500 μm^2. Samples F and G are the nonwoven surgical and N95 masks, respectively, having relatively small, irregularly shaped pores compared to samples B, C, D, and E (Figures 2b and S6). The pore size distribution of sample A was comparable to that of N95 (sample G), where the maximum pore size overserved was 8250 μm^2 (Figure 2c). It has been inferred from Figure 2c that sample G would be the best in terms of protection, as most of the smaller size droplets (distribution of which is denoted by black dotted line), which came onto the surface of the N95 mask, were less likely to pass through it. This is because the maximum pore size, as well as the density of the pores of any particular size on this mask, was smaller compared

https://doi.org/10.1021/acsabm.1c00851
ACS Appl. Bio Mater. XXXX, XXX, XXX−XXX

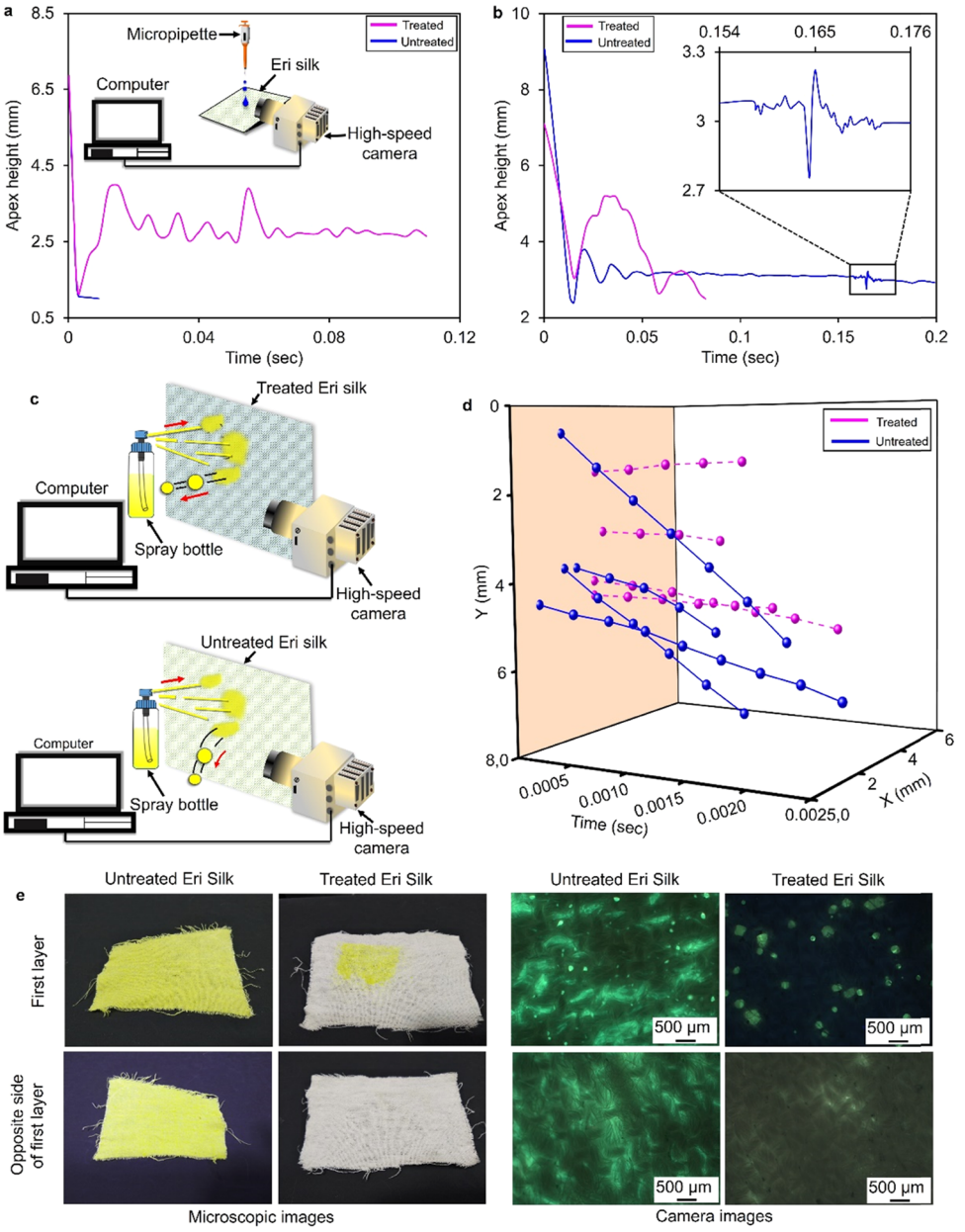

Figure 3. Droplet behavior on treated and untreated Eri silk mask. (a) Behavior of a 10 μL droplet when it was dropped on a slanted silk surface from a height of 33 cm (high impact). The angle of the slope was 15° to the horizontal axis. The inset shows the experimental setup for the same. The plot shows the droplet apex height trail with time on as-purchased (blue line) and OTS-treated (pink line) Eri silk fabric surfaces, respectively. (b) Results from the experiment, similar to that in (a), but the droplet fell from a relatively shorter height of 5 cm (low impact) on as-purchased (blue line) and OTS-treated (pink line) Eri silk fabric surfaces, respectively. The inset graph shows the behavior when the droplet had transformed from Cassie-impregnated Wenzel state to Wenzel state on the as-purchased Eri silk fabric surface (see text for details). (c) Experimental setup to capture the droplets bouncing back from vertically placed treated (top) and as-purchased (bottom) Eri silk upon spraying from 5 cm distance. The droplets bouncing back from treated Eri silk initially traveled faster in a straighter path, whereas the as-purchased Eri silk followed a curved downward path due to the lower velocity experienced by the droplets. (d) Plot showing the trajectories of typical droplets bouncing back from the vertically placed as-purchased (blue) and OTS-treated (pink) Eri silk fabric as shown in (c) after hitting the surface. (e) Optical and fluorescence microscopic images of both as-purchased and OTS-treated Eri silk cloth pieces (front surface and back surface) after spraying with the liquid dye as depicted in (c).

to the density of the droplets of that particular size. Similarly, cloth 1 (sample A) was also expected to have better performance in terms of droplet penetration. However, due to the high liquid absorption capacity, the use of this mask may not be advisable. On the other hand, Mask C (Muga silk) has a considerable number of larger pores (with the largest pore size observed being 72 500 μm^2) with respect to the small droplets hitting the surface (Figure 2c). This would lead to a significant amount of droplet penetration through the mask layer. After the treatment with OTS, the largest pore size of sample D1 was reduced by some extent to 31 000 μm^2 compared to unmodified sample D with 37 500 μm^2 (Figure 2c). The reduction in pore size for sample D1 would block smaller droplets more in numbers coming toward it than sample D. The pore size distribution of D1 revealed that after OTS treatment, the mask prevented relatively larger droplets from

https://doi.org/10.1021/acsabm.1c00851
ACS Appl. Bio Mater. XXXX, XXX, XXX−XXX

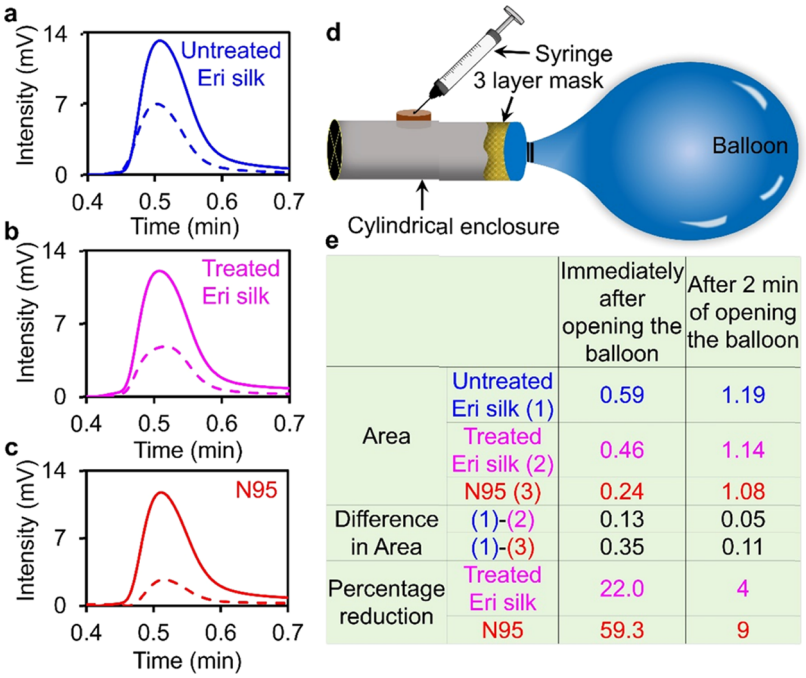

		Immediately after opening the balloon	After 2 min of opening the balloon
Area	Untreated Eri silk (1)	0.59	1.19
	Treated Eri silk (2)	0.46	1.14
	N95 (3)	0.24	1.08
Difference in Area	(1)-(2)	0.13	0.05
	(1)-(3)	0.35	0.11
Percentage reduction	Treated Eri silk	22.0	4
	N95	59.3	9

Figure 4. Breathability of N95, as-purchased, and treated Eri silk masks. Graphs showing the gas chromatography (GC) peak of oxygen after passing through the three layers of mask materials: for (a) as-purchased Eri silk, (b) OTS-treated Eri silk, and (c) N95 mask fabrics. Dashed and solid lines show the oxygen peaks immediately after the opening of the oxygen-containing balloon and after 2 min of opening, respectively. The time on the *x*-axis is the residence time for the detection of oxygen by the GC machine. (d) Experimental setup showing how oxygen was collected from a cylindrical enclosure for gas chromatographic detection. (e) Table showing the area under the curve for the plots in (a–c) depicting the permeability (breathability) of oxygen through the three-layered masks and percentage reduction of the breathability with respect to the as-purchased Eri silk mask fabric.

penetration that was similar to that of a surgical mask and also was better than a surgical mask for small-size droplets. Next, we will focus our discussion on OTS-treated mask (D1) and its behavior with droplet impact and its breathability compared to the untreated mask (D).

The spherical SARS-CoV-2 viruses with spikes are usually 120 nm in diameter.[39] Droplets ranging from 1 to 200 μm in diameter are considered to be airborne.[40] The viruses aggregated into clusters are cited to be potentially transmitted via droplets of diameter 20 μm.[41] Taking this as an instance, from Figure 2c, we could clearly see that the N95 mask was very efficient in blocking these model droplets. As this mask has smaller counts for pore size in the range of 200–400 μm^2, it could typically block droplets having an area of approximately 400 μm^2. Although the largest pore size available in the N95 was noticed as 8250 μm^2, a minimal amount of smaller-sized droplets would definitely pass through the meshes. Similarly, when samples D and D1 were extrapolated (represented by orange and blue dotted lines respectively in Figure 2c), D1 was seen to have a smaller pore size compared to D and almost comparable to N95 in performance in resisting deposition and/or penetration of such model droplets.

2.3. Droplet Impact on a Treated Mask. An experiment was carried out to examine the impact behavior of a 10 μL aqueous glycerol (60%) droplet when dropped from a height of ~33 cm (emulating high impact) and ~5 cm (emulating low impact) on an unmodified Eri silk and OTS-treated hydrophobic Eri silk. A single layer of the test silk sample was tightly clamped to a custom-made holder and kept at an inclination of 15° to the horizontal axis. To detect whether the liquid was absorbed by the fabric or not, the fluorescein Na salt dye was mixed with the aqueous glycerol and used for this experiment. A high-speed camera (Phantom VEO E-340L model, 5600 fps, 1024 × 500 resolution) was used to capture the impact events. Interestingly, for the high-impact experiments, the droplet falling on the unmodified silk sieved through the fabric in 9 ms (see SI Video 1). On the other hand, for the OTS-treated hydrophobic Eri silk, the droplet did not pass through the fabric (SI Video 2). Due to the high impact, the parent droplet after hitting the treated silk first fragmented into smaller daughter droplets and the remaining parent droplet adhered to the surface of the fabric, which oscillated on the surface with diminishing amplitude, and eventually evaporated after a long time (50 min) leaving a trace of the dye on the front surface of the fabric only (SI Video 2 and Figure S9). The trajectory of the apex of the falling parent droplet was tracked and is shown in Figure 3a. The liquid dye did not get absorbed by the fabric, which was apparent from the cleanliness of the back side of the fabric (Supporting information Figure S9) at the end of the experiment. On the other hand, the unmodified Eri silk completely soaked the dye droplet and both the front and back side of the fabric became yellow spanning over the large area (Figure 3e).

A similar experiment with a droplet falling from a height of ~5 cm (low impact) showed that the droplet was stuck on the untreated surface with diminishing oscillation. The trajectory of the apex of the falling droplet was tracked and is depicted by the blue line in Figure 3b. The droplet was stuck into a low-energy "Cassie-impregnated Wenzel state"[42,43] due to the impact on the microprojections and secondary micro/nanofolds on the fabric surface. The droplet initially wetted the large micropits, but as the water could not penetrate further into the smaller micro/nanofolds, it created small air pockets.

https://doi.org/10.1021/acsabm.1c00851
ACS Appl. Bio Mater. XXXX, XXX, XXX–XXX

These air pockets helped to retain the droplet into the Cassie-impregnated Wenzel state for some time. The droplet oscillation at this state completely diminishes after ~70 ms, and at ~150 ms, the droplet transited to the relatively lower-energy "Wenzel" state associated with the fluctuation of the droplet again (see fluctuation in the inset of Figure 3b) (see SI Video 3). Importantly, on the treated hydrophobic silk surface, upon impact, droplets bounced back to the air completely and eventually rolled down the surface without leaving any trace of the liquid or dye (see SI Video 4). The trajectory of the drop apex is shown by the pink line in Figure 3b. To emulate a more realistic scenario of the mask−droplet interaction, the dyed liquid was sprayed on a vertically placed unmodified and treated Eri silk surface from a distance of ~5 cm. The schematic of this experiment is shown in Figure 3c. The droplet bouncing velocities from such surfaces was estimated from the trajectories tracked with the high-speed camera (at 3200 fps) (Figure 3d) (see SI Videos 5 and 6 in the Supporting Information). It was found that most of the droplets bounced back with a high average horizontal velocity (~702.6 mm/s) from the treated hydrophobic surface. However, from the untreated hydrophilic Eri silk, the droplet bounced back with an average horizontal velocity (~247.0 mm/s) that was much lower than the same from the hydrophobic surface and with a relatively faster downward fall (Figure 3d). It was also noticed that fewer droplets bounced back from the untreated Eri silk in the initial period than the treated Eri silk. While spraying, a continuous liquid film started forming on the untreated surface from 4 s onward due to which the droplets collided with the liquid film and splashed out as droplets of different sizes (SI Video 5). However, hydrophobicity of treated Eri silk resulted in no liquid film formation during the initial period of spraying (SI Video 6).

Optical images and fluorescence microscope images of the unmodified and treated Eri silk showed (Figure 3e) that the dye was absorbed completely by the threads of the untreated Eri silk, whereas only the front surface of the hydrophobic Eri silk demonstrated a minimum deposition of the dye from the evaporated liquid.

2.4. Breathability of the Treated Mask. To check the breathability of three-layered mask materials, we checked oxygen permeability through them. The sample fabric (as-purchased Eri silk, treated hydrophobic Eri silk, and N95) was first wrapped on the open mouth of a cylindrical enclosure having a sealed rubber stopper at the side of the cylinder. In each experiment, three layers of the test fabric sample were used. A balloon filled with ~0.5 L of oxygen at room temperature (23 °C) and pressure (1 atm) was tightly tied to the open mouth of the cylinder having the fabric sample to avoid any leakage of oxygen.

When the tie was opened, the oxygen permeated through the fabric sample and gradually increased the oxygen concentration inside the cylinder. The gas was collected from the cylinder through the sealed rubber stopper using a syringe (Figure 4d), and gas chromatography (GC) was used to estimate the concentration of the oxygen inside the cylinder. The gas was collected from the cylinder immediately after opening the balloon (dashed lines in Figure 4a−c) and after 2 min of opening the balloon (solid lines in Figure 4a−c). The GC curves, shown in Figure 4a−c, have values presented after subtraction of the background oxygen that was present before the opening of the balloon. The results shown in tabular form in Figure 4e revealed that immediate breathability (i.e., immediately following the opening of the oxygen source) of the Eri silk was maximum and that was reduced by ~22% after OTS treatment. However, compared to untreated Eri silk, the breathability of N95 was much less (~59%). For longer-duration breathability (after 2 min of the opening of oxygen source), these reductions for treated Eri silk and N95 were ~4% and ~9%, respectively. Nevertheless, immediate breathability should be the primary concern while choosing an appropriate mask material. Here, the comparison was performed based on untreated, as-purchased Eri silk mask as among these samples, as Eri silk mask (both OTS-treated and as-purchased fabrics) have been the most comfortable and easy to breathe through it.

Another important study on droplet penetration through the mask was performed to emulate the contamination of a nearby person while a masked infected patient is sneezing or coughing. For this, we kept two masks of the same materials in close proximity (about 1 cm apart), and dyed aqueous glycerol (60% by volume) was sprayed through one of the masks (mask 1). After spraying, the other mask (mask 2) surface was observed under the fluorescence microscope to check the depositions (see Figure S10 in the Supporting Information). The results revealed that mask 1 when sprayed with liquid may have led to the transmission of the liquid to the nearby mask 2 predominantly by direct droplet penetration through mask 1 and maybe to some extent by diffusion from liquid-laden mask 1 to pristine mask 2. Due to the larger pore size of Muga silk (sample C), the droplets could pass through the pores and showed the highest deposition of 61% of the dye on mask 2, whereas N95 (sample G) showed the minimum deposition of 0.06% on mask 2 possibly due to its small pore size.

3. CONCLUSIONS

In this work, we have investigated the performance of cloth, silk, surgical, and N95 masks primarily in terms of their capability to absorb liquid droplets that were sprayed upon the fabrics. It was found that N95 and surgical masks were among the least liquid-absorbing masks with less fractional area coverage by the droplets on the outer layer of the mask. On the other hand, the hydrophilic cloth was found to have the highest capability to absorb liquid with the fractional area covered by the incoming droplets >35%. Although the N95 mask was the best, it had poor breathability, unlike a comfortable cloth mask. As a recent article[23] indicated that the SARS-CoV-2 virus is airborne, the liquid absorption capability of a mask is a topic of great concern. Masks having a high capability of absorption of liquid can be the source of plausible infection. The situation becomes more detrimental if the mask is poorly breathable as this may induce oxygen deficiency in the bloodstream of a patient due to lack of air passing through the mask. This would induce strong inhalation, which may help carry pathogens inward through the layers of the mask from the outer layers of the liquid-laden mask. Thus, it would be better to have a reasonably breathable mask having low liquid absorption capability. In this direction, we have modified a hydrophilic mask (Eri silk) to a robust hydrophobic breathable mask using a nanometer-thick coating of OTS. The mask fabric exhibited low liquid absorption capability even at the high impact of (aqueous) liquid drops. The droplets hitting the outer layer of the modified Eri silk fabric repelled off, which prevented deposition of the droplet on its surface. Wearing a three-layered modified hydrophobic Eri silk mask might be sufficient to reduce the chance of being

https://doi.org/10.1021/acsabm.1c00851
ACS Appl. Bio Mater. XXXX, XXX, XXX−XXX

infected or spreading an infection to others. Along with the top hydrophobic layer prescribed in this work, one can also use multifunctional inner layers such as active antibacterial coating[44] and intermediate electrostatic layers[45] for better protection against airborne pathogens such as SARS-CoV-2.

4. MATERIALS AND METHODS

4.1. Types of Masks. In this study, we considered four different types, namely, N95 mask (manufactured by E-Spin Nanotech Pvt. Ltd., India), surgical mask (locally procured), cloth masks (locally procured), and silk masks (locally procured). We have considered the masks for study in this report based on their ease of accessibility to a large populace such as cotton mask (Cloth 1 and Cloth 2), silk mask (Muga silk, Eri silk, and Paat (Mulberry) silk), surgical mask, and N95 mask (Table 1). Cloth masks i.e., cotton, polyester, or silk varieties, are easily available and are also cost-effective. All of the above-mentioned masks are being used by people for protection from airborne infections and pollution. The Muga silk is produced from a wild silkworm *Antheraea assamensis* from Assam, located in the north-eastern region of India.[46] Eri silk comes from the caterpillar *Samia ricini* that is regional to northeast India and some parts of China and Japan.[47] Paat silk also known as Mulberry silk comes from silkworm *Bombyx textor*, which feeds on mulberry leaves.[48]

4.2. Materials. Human mucus[49] is more viscous than water. To mimic the viscosity of mucus, 60% v/v glycerol solution was used to carry out the experiments. For clear detection of the droplets on the mask surface and its absorption on the fabric under fluorescence microscopy, fluorescein sodium salt (dissolved in the solution mentioned above) was used as the marker.

4.3. Experimental Setup. All of the experiments were carried out in a closed cuboidal chamber of approximate dimensions 30 cm × 16 cm × 15 cm. Two 4 cm × 4 cm windows were cut out on the opposite faces with respect to the box's length. On one window, a mask fabric was fixed with the outer side of the mask fabric facing the inside of the box. On the opposite, a spray bottle was placed containing the glycerol solution as shown in Figure 1a. After placing the sample, the spray bottle was pressed twice, and then the sample was observed under a fluorescence microscope.

4.4. Preparation of Octadecyltrichlorosilane (OTS) Solution. OTS is used extensively as a surface-modifying chemical because of its fluorine-free composition, which makes it both nonhazardous to health and the environment.[50,51] The OTS solution was prepared by mixing 20 μL of octadecyltrichlorosilane (OTS) in 10 mL of toluene.[52] The mixer solution was stirred for 10 min and then heated on a hot plate at 60 °C for 30 min. After that, the solution was cooled to room temperature for some time before being used for further experiment.

4.5. Preparation of Hydrophobic Eri Silk. The procured Eri silk fabric was first washed with detergent to remove the excess dirt or oil present in it and then dried naturally under the sun. The dried silk pieces were first washed with acetone for 1 min to remove any excess detergent stuck to the fabric. Subsequently, they were washed in DI water for 2 min to remove the acetone. First, it was dried with nitrogen gas to remove the excess water. Once the cloth pieces become moist, they were dried in a hot-air oven at around 100 °C for 10 min until complete drying. After that, UV-ozone treatment was done for 2 min in the UV-ozone chamber (Novascan Technologies, model: PSD UV4) and the fabric was immediately transferred to the OTS solution[52] prepared (several pieces of them). After keeping the cloth pieces in the solution for 30 min, they were washed with toluene to remove the excess OTS present on the fiber. Then, the pieces were dried with nitrogen and finally kept in a hot-air oven at 80 °C for 10 min. The plausible chemical reaction of OTS with the fabric (Figure S1B in the Supporting Information) showed that the Si molecules of OTS formed chemical bonds with the −OH groups of the fabric and the long hydrocarbon chains of the OTS dangled outside in the air. The dangled hydrocarbon chains are not harmful, and thus the OTS-treated silk masks are safe for human use.

Typically, a 2−3 nm[53] OTS layer is known to form on the surface of Si, which may well be the case here that rendered the silk hydrophobic (sample D1). The thickness of the deposited OTS layer was measured with an ellipsometer. As laser light interacts with cloth fabric, thickness measurement on cloth was not feasible. Moreover, the conformal topography formed by the thin layer of coated OTS over the textured silk fabric made the ellipsometric measurements difficult over the cloth.[54] Instead, cleaned silicon wafer was ozone-treated for 30 min followed by a 30 min OTS treatment and then measured with an ellipsometer for thickness as an alternative. The thickness of the OTS layer was measured to be 1.9 ± 0.1 nm with a root-mean-square error (RMSE) of 0.585 (the operating data used in the ellipsometer are provided in the Supporting information, SI). The coating of the silk by OTS was confirmed by Fourier transform infrared (FTIR) spectroscopy with characteristic peaks of the compound being present in the spectrum as shown in Figure S2 (Supporting Information). The FTIR data were supported by the presence of the Si on the treated Eri silk captured in the EDS analysis (Figure S3 in the Supporting Information). The hydrophobicity of the treated Eri silk was maintained even after three times washing with detergent. At room temperature, the samples were dipped inside commercially available laundry detergent solution and, at the same time, the fabric surface was rubbed six times with fingers inside the detergent solution. The fabric was again cleaned with only water to remove the detergent and dried first with N_2 gas followed by heating on a hot plate at around 80 °C for 5 min. After washing and drying, the water droplets falling on the treated Eri silk were seen to be rolling away as before from the surface without wetting the silk.

4.6. Quantitative Analysis. All images from the fluorescence microscope (Carl Zeiss, Model A1MAT HAL 100) were analyzed in an open-source software "ImageJ" for measurement of the area covered by the droplets on the surface of the mask. The quantitative measurements were done in "Microsoft Excel" and "Origin." In "ImageJ" software, we can adjust the image with threshold function and then analyze and measure the area of the image with ROI Manager function. In "Origin" software with the frequency count function, we can find the normalized probability distribution of the pore area of the mask. The contact angle measurements for all of the samples were done with the help of the contact angle goniometer (Holmarc Opto-Mechatronics, model: HO-IAD-CAM-01B). To have better clarity about the spatial arrangement of the fibers on all masks, field emission scanning electron microscopy (FESEM) (JSM 7610 F, JEOL, Japan) was also performed. EDS analysis of the treated and pristine Eri silk was performed using FESEM with an EDS detector (Zeiss, model: Sigma 300).

■ ASSOCIATED CONTENT

Supporting Information

The Supporting Information is available free of charge at https://pubs.acs.org/doi/10.1021/acsabm.1c00851.

Types of mask used and chemical modification of hydrophilic Eri silk into the hydrophobic nature, ellipsometer operating data, Fourier transform infrared spectroscopy−attenuated total reflectance (FTIR-ATR) spectra, contact angle vs. fractional area coverage, field emission scanning electron microscopy−energy-dispersive spectroscopy (FESEM-EDS) of as-purchased and OTS-treated Eri silk fabric, fluorescence microscopy images of masks with absorbed dye, fractional area coverage at different distances, OTS treatment of cotton cloth 1 (sample A), percentage decrease in fractional area coverage at 1.8 m with reference to 0.3 m, optical micrographs of the first layer of masks, FESEM images of the first layer of masks, pore size distribution of masks, droplet's impression on treated Eri silk fabric, and penetration and soaking capacity of the masks (PDF)

https://doi.org/10.1021/acsabm.1c00851
ACS Appl. Bio Mater. XXXX, XXX, XXX−XXX

high-impact droplet falling on an inclined as-purchased Eri silk (Video 1) (MP4)
high-impact droplet falling on inclined OTS-treated hydrophobic Eri silk (Video 2) (MP4)
low-impact droplet falling on an inclined as-purchased Eri silk (Video 3) (MP4)
low-impact droplet falling on inclined OTS-treated hydrophobic Eri silk (Video 4) (MP4)
liquid spray at the vertical as-purchased Eri silk (Video 5) (MP4)
liquid spray at the vertical OTS-treated hydrophobic Eri silk (Video 6) (MP4)

AUTHOR INFORMATION

Corresponding Authors

Arun Chattopadhyay − *Department of Chemistry and Centre for Nanotechnology, Indian Institute of Technology Guwahati, Guwahati, Assam 781039, India;* orcid.org/0000-0001-5095-6463; Email: arun@iitg.ac.in

Partho Sarathi Gooh Pattader − *Department of Chemical Engineering, Centre for Nanotechnology, and School of Health Science and Technology, Indian Institute of Technology Guwahati, Guwahati, Assam 781039, India;* orcid.org/0000-0002-8818-0741; Email: psgp@iitg.ac.in

Authors

Prerona Gogoi − *Department of Chemical Engineering, Indian Institute of Technology Guwahati, Guwahati, Assam 781039, India*

Sunil Kumar Singh − *Department of Chemical Engineering, Indian Institute of Technology Guwahati, Guwahati, Assam 781039, India*

Ankur Pandey − *Department of Chemical Engineering, Indian Institute of Technology Guwahati, Guwahati, Assam 781039, India*

Complete contact information is available at: https://pubs.acs.org/10.1021/acsabm.1c00851

Author Contributions

A.C. and P.S.G.P. conceived and designed the experiments. P.G. performed most of the experiments. S.K.S. and A.P. helped in some of the experiments and characterizations. Results were analyzed by P.G., A.C., and P.S.G.P. All of the authors contributed to the final version of the manuscript.

Notes

The authors declare no competing financial interest.

ACKNOWLEDGMENTS

P.S.G.P. thanks the analytical facility of the Department of Chemical Engineering, IITG; CIF, IITG; DST SERB, Grant no. CRG/2019/000118, and FIST, DST, Grant no. SR/FST/ETII-071/2016(G). A.C. thanks the Department of Science and Technology for the J. C. Bose fellowship (JCB/2019/000039). The authors thank MeitY (grant no. 5(9)/2012-NANO) for financial aids.

REFERENCES

(1) Chu, D. K.; Akl, E. A.; Duda, S.; Solo, K.; Yaacoub, S.; Schünemann, H. J.; El-harakeh, A.; Bognanni, A.; Lotfi, T.; Loeb, M.; Hajizadeh, A.; Bak, A.; Izcovich, A.; Cuello-Garcia, C. A.; Chen, C.; Harris, D. J.; Borowiack, E.; Chamseddine, F.; Schünemann, F.; Morgano, G. P.; Muti Schünemann, G. E. U.; Chen, G.; Zhao, H.; Neumann, I.; Chan, J.; Khabsa, J.; Hneiny, L.; Harrison, L.; Smith, M.; Rizk, N.; Giorgi Rossi, P.; AbiHanna, P.; El-khoury, R.; Stalteri, R.; Baldeh, T.; Piggott, T.; Zhang, Y.; Saad, Z.; Khamis, A.; Reinap, M. Physical Distancing, Face Masks, and Eye Protection to Prevent Person-to-Person Transmission of SARS-CoV-2 and COVID-19: A Systematic Review and Meta-Analysis. *Lancet* **2020**, *395*, 1973−1987.

(2) Brooks, J. T.; Butler, J. C. Effectiveness of Mask Wearing to Control Community Spread of SARS-CoV-2. *JAMA* **2021**, *325*, 998−999.

(3) Organization, W. H. Mask Use in the Context of COVID-19: Interim Guidance, 1 December 2020. https://apps.who.int/iris/bitstream/handle/10665/337199/WHO-2019-nCov-IPC_Masks-2020.5-eng.pdf?sequence=1&isAllowed=y (accessed Sep 05, 2021).

(4) Dugdale, C. M.; Walensky, R. P. Filtration Efficiency, Effectiveness, and Availability of N95 Face Masks for COVID-19 Prevention. *JAMA Intern. Med.* **2020**, *180*, 1612−1613.

(5) Roberge, R. J.; Bayer, E.; Powell, J. B.; Coca, A.; Roberge, M. R.; Benson, S. M. Effect of Exhaled Moisture on Breathing Resistance of N95 Filtering Facepiece Respirators. *Ann. Occup. Hyg.* **2010**, *54*, 671−677.

(6) Yue, Y.; Wang, J.; He, W.; Guo, Y.; Gao, H.; Liu, J. Evaluation of Regeneration Processes for Filtering Facepiece Respirators in Terms of the Bacteria Inactivation Efficiency and Influences on Filtration Performance. *ACS Nano* **2020**, *14*, 13161−13171.

(7) Aydin, O.; Emon, B.; Cheng, S.; Hong, L.; Chamorro, L. P. Performance Offabrics for Home-Made Masks against the Spread of COVID-19 through Droplets: A Quantitative Mechanistic Study. *Extrem. Mechnics Lett.* **2020**, *40*, No. 100924.

(8) Wibisono, Y.; Fadila, C. R.; Saiful, S.; Bilad, M. R. Facile Approaches of Polymeric Face Masks Reuse and Reinforcements for Micro-Aerosol Droplets and Viruses Filtration: A Review. *Polymers* **2020**, *12*, No. 2516.

(9) Tan, N. P. B.; Paclijan, S. S.; Ali, H. N. M.; Hallazgo, C. M. J. S.; Lopez, C. J. F.; Ebora, Y. C. Solution Blow Spinning (SBS) Nanofibers for Composite Air Filter Masks. *ACS Appl. Nano Mater.* **2019**, *2*, 2475−2483.

(10) Shen, H.; Zhou, Z.; Wang, H.; Zhang, M.; Han, M.; Durkin, D. P.; Shuai, D.; Shen, Y. Development of Electrospun Nanofibrous Filters for Controlling Coronavirus Aerosols. *Environ. Sci. Technol. Lett.* **2021**, *8*, 545−550.

(11) Bayersdorfer, J.; Giboney, S.; Martin, R.; Moore, A.; Bartles, R. Novel Manufacturing of Simple Masks in Response to International Shortages: Bacterial and Particulate Filtration Efficiency Testing. *Am. J. Infect. Control* **2020**, *48*, 1543−1545.

(12) Chua, M. H.; Cheng, W.; Goh, S. S.; Kong, J.; Li, B.; Lim, J. Y. C.; Mao, L.; Wang, S.; Xue, K.; Yang, L.; Ye, E.; Zhang, K.; Cheong, W. C. D.; Tan, B. H.; Li, Z.; Tan, B. H.; Loh, X. J. Face Masks in the New COVID-19 Normal: Materials, Testing, and Perspectives. *Research* **2020**, *2020*, 1−40.

(13) Parlin, A. F.; Stratton, S. M.; Culley, T. M.; Guerra, P. A. A Laboratory-Based Study Examining the Properties of Silk Fabric to Evaluate Its Potential as a Protective Barrier for Personal Protective Equipment and as a Functional Material for Face Coverings during the COVID-19 Pandemic. *PLoS One* **2020**, *15*, No. e0239531.

(14) Rengasamy, S.; Eimer, B.; Shaffer, R. E. Simple Respiratory Protection - Evaluation of the Filtration Performance of Cloth Masks and Common Fabric Materials against 20-1000 Nm Size Particles. *Ann. Occup. Hyg.* **2010**, *54*, 789−798.

(15) Borah, M. P.; Jose, S.; Kalita, B. B.; Shakyawar, D. B.; Pandit, P. Water Repellent Finishing on Eri Silk Fabric Using Nano Silica. *J. Text. Inst.* **2020**, *111*, 701−708.

(16) Gogoi, D.; Choudhury, A. J.; Chutia, J.; Pal, A. R.; Dass, N. N.; Devi, D.; Patil, D. S. Enhancement of Hydrophobicity and Tensile Strength of Muga Silk Fiber by Radiofrequency Ar Plasma Discharge. *Appl. Surf. Sci.* **2011**, *258*, 126−135.

(17) Konda, A.; Prakash, A.; Moss, G. A.; Schmoldt, M.; Grant, G. D.; Guha, S. Aerosol Filtration Efficiency of Common Fabrics Used in Respiratory Cloth Masks. *ACS Nano* **2020**, *14*, 6339−6347.

(18) Arumuru, V.; Pasa, J.; Samantaray, S. S.; Varma, V. S. Breathing, Virus Transmission, and Social Distancing—An Experimental Visualization Study. *AIP Adv.* **2021**, *11*, No. 045205.
(19) Arumuru, V.; Pasa, J.; Samantaray, S. S. Experimental Visualization of Sneezing and Efficacy of Face Masks and Shields. *Phys. Fluids* **2020**, *32*, No. 115129.
(20) Sharma, S.; Pinto, R.; Saha, A.; Chaudhuri, S.; Basu, S. On Secondary Atomization and Blockage of Surrogate Cough Droplets in Single- And Multilayer Face Masks. *Sci. Adv.* **2021**, *7*, No. eabf0452.
(21) Fischer, E. P.; Fischer, M. C.; Grass, D.; Henrion, I.; Warren, W. S.; Westman, E. Low-Cost Measurement of Face Mask Efficacy for Filtering Expelled Droplets during Speech. *Sci. Adv.* **2020**, *6*, No. eabd3083.
(22) Bałazy, A.; Toivola, M.; Adhikari, A.; Sivasubramani, S. K.; Reponen, T.; Grinshpun, S. A. Do N95 Respirators Provide 95% Protection Level against Airborne Viruses, and How Adequate Are Surgical Masks? *Am. J. Infect. Control* **2006**, *34*, 51−57.
(23) Greenhalgh, T.; Jimenez, J. L.; Prather, K. A.; Tufekci, Z.; Fisman, D.; Schooley, R. Ten Scientific Reasons in Support of Airborne Transmission of SARS-CoV-2. *Lancet* **2021**, *397*, 1603−1605.
(24) Tcharkhtchi, A.; Abbasnezhad, N.; Zarbini Seydani, M.; Zirak, N.; Farzaneh, S.; Shirinbayan, M. An Overview of Filtration Efficiency through the Masks: Mechanisms of the Aerosols Penetration. *Bioact. Mater.* **2021**, *6*, 106−122.
(25) Akalin, M.; Usta, I.; Kocak, D.; Ozen, M. S. Investigation of the Filtration Properties of Medical Masks. In *Woodhead Publishing Series in Textiles*, Anand, S. C.; Kennedy, J. F.; Miraftab, M.; Rajendran, S. B. T.-M.; H, T., Eds.; Woodhead Publishing, 2010; pp 93−97.
(26) Liao, L.; Xiao, W.; Zhao, M.; Yu, X.; Wang, H.; Wang, Q.; Chu, S.; Cui, Y. Can N95 Respirators Be Reused after Disinfection? How Many Times? *ACS Nano* **2020**, *14*, 6348−6356.
(27) Larsen, G. S.; Cheng, Y.; Daemen, L. L.; Lamichhane, T. N.; Hensley, D. K.; Hong, K.; Meyer, H. M.; Monaco, S. J.; Levine, A. M.; Lee, R. J.; Betters, E.; Sitzlar, K.; Heineman, J.; West, J.; Lloyd, P.; Kunc, V.; Love, L.; Theodore, M.; Paranthaman, M. P. Polymer, Additives, and Processing Effects on N95 Filter Performance. *ACS Appl. Polym. Mater.* **2021**, *3*, 1022−1031.
(28) Pandey, L. K.; Singh, V. V.; Sharma, P. K.; Meher, D.; Biswas, U.; Sathe, M.; Ganesan, K.; Thakare, V. B.; Agarwal, K. Screening of Core Filter Layer for the Development of Respiratory Mask to Combat COVID-19. *Sci. Rep.* **2021**, *11*, No. 10187.
(29) Bhattacharjee, S.; Joshi, R.; Yasir, M.; Adhikari, A.; Chughtai, A. A.; Heslop, D.; Bull, R.; Willcox, M.; Macintyre, C. R. Graphene- and Nanoparticle-Embedded Antimicrobial and Biocompatible Cotton/Silk Fabrics for Protective Clothing. *ACS Appl. Bio. Mater.* **2021**, *4*, 6175−6185.
(30) Huang, J. T.; Huang, V. J. Evaluation of the Efficiency of Medical Masks and the Creation of New Medical Masks. *J. Int. Med. Res.* **2007**, *35*, 213−223.
(31) Kang, P. K.; Shah, D. O. Filtration of Nanoparticles with Dimethyldioctadecylammonium Bromide Treated Microporous Polypropylene Filters. *Langmuir* **1997**, *13*, 1820−1826.
(32) McCarty, L. S.; Whitesides, G. M. Electrostatic Charging Due to Separation of Ions at Interfaces: Contact Electrification of Ionic Electrets. *Angew. Chem., Int. Ed.* **2008**, *47*, 2188−2207.
(33) Li, Y.; Yin, X.; Si, Y.; Yu, J.; Ding, B. All-Polymer Hybrid Electret Fibers for High-Efficiency and Low-Resistance Filter Media. *Chem. Eng. J.* **2020**, *398*, No. 125626.
(34) Lee, K. W.; Liu, B. Y. H. On the Minimum Efficiency and the Most Penetrating Particle Size for Fibrous Filters. *J. Air Pollut. Control Assoc.* **1980**, *30*, 377−381.
(35) Bhattacharjee, S.; Bahl, P.; Chughtai, A. A.; MacIntyre, C. R. Last-Resort Strategies during Mask Shortages: Optimal Design Features of Cloth Masks and Decontamination of Disposable Masks during the COVID-19 Pandemic. *BMJ Open Respir. Res.* **2020**, *7*, No. e000698.
(36) Hinds, W. C. *Aerosol Technology: Properties, Behaviour, and Measurement of Airborne Particles*, 2nd ed.; Wiley: New York (N.Y.), 1999.
(37) Bhattacharjee, S.; Bahl, P.; de Silva, C.; Doolan, C.; Chughtai, A. A.; Heslop, D.; Macintyre, C. R. Experimental Evidence for the Optimal Design of a High-Performing Cloth Mask. *ACS Biomater. Sci. Eng.* **2021**, *7*, 2791−2802.
(38) Bhattacharjee, S.; Macintyre, C. R.; Bahl, P.; Kumar, U.; Wen, X.; Chughtai, A. A.; Joshi, R.; et al. Reduced Graphene Oxide and Nanoparticles Incorporated Durable Electroconductive Silk Fabrics. *Adv. Mater. Interfaces* **2020**, *7*, No. 2000814.
(39) Wood, B. R.; Kochan, K.; Bedolla, D. E.; Salazar-Quiroz, N.; Grimley, S.; Perez-Guaita, D.; Baker, M. J.; Vongsvivut, J.; Tobin, M.; Bambery, K.; Christensen, D.; Pasricha, S.; Eden, A. K.; Mclean, A.; Roy, S.; Roberts, J.; Druce, J.; Williamson, D. A.; McAuley, J.; Catton, M.; Purcell, D.; Godfrey, D.; Heruad, P. Infrared Based Saliva Screening Test for COVID-19. *Angew. Chem. Int. Ed.* **2021**, *60*, 17102−17107.
(40) Vuorinen, V.; Aarnio, M.; Alava, M.; Alopaeus, V.; Atanasova, N.; Auvinen, M.; Balasubramanian, N.; Bordbar, H.; Erästö, P.; Grande, R.; Hayward, N.; Hellsten, A.; Hostikka, S.; Hokkanen, J.; Kaario, O.; Karvinen, A.; Kivistö, I.; Korhonen, M.; Kosonen, R.; Kuusela, J.; Lestinen, S.; Laurila, E.; Nieminen, H. J.; Peltonen, P.; Pokki, J.; Puisto, A.; Råback, P.; Salmenjoki, H.; Sironen, T.; Österberg, M. Modelling Aerosol Transport and Virus Exposure with Numerical Simulations in Relation to SARS-CoV-2 Transmission by Inhalation Indoors. *Saf. Sci.* **2020**, *130*, No. 104866.
(41) Anand, S.; Mayya, Y. S. Size Distribution of Virus Laden Droplets from Expiratory Ejecta of Infected Subjects. *Sci. Rep.* **2020**, *10*, No. 21174.
(42) Ghosh, U. U.; Nair, S.; Das, A.; Mukherjee, R.; Dasgupta, S. Replicating and Resolving Wetting and Adhesion Characteristics of a Rose Petal. *Colloids Surf., A* **2019**, *561*, 9−17.
(43) Roy, D.; Pandey, K.; Banik, M.; Mukherjee, R.; Basu, S. Dynamics of Droplet Impingement on Bioinspired Surface: Insights into Spreading, Anomalous Stickiness and Break-Up. *Proc. R. Soc. A* **2019**, *475*, No. 20190260.
(44) Kharaghani, D.; Khan, M. Q.; Shahrzad, A.; Inoue, Y.; Yamamoto, T.; Rozet, S.; Tamada, Y.; Kim, I. S. Preparation and In-Vitro Assessment of Hierarchal Organized Antibacterial Breath Mask Based on Polyacrylonitrile/Silver (PAN/AgNPs) Nanofiber. *Nanomaterials* **2018**, *8*, No. 461.
(45) Martin, S. B.; Moyer, E. S. Electrostatic Respirator Filter Media: Filter Efficiency and Most Penetrating Particle Size Effects. *Appl. Occup. Environ. Hyg.* **2000**, *15*, 609−617.
(46) Devi, D.; Sarma, N.; Sen; Talukdar, B.; Chetri, P.; Dass, N. N. Study of the Structure of Degummed *Antheraea Assamensis* (Muga) Silk Fibre. *J. Text. Inst.* **2011**, *102*, 527−533.
(47) Xue, Y.; Wang, F.; Torculas, M.; Lo, S.; Hu, X. Formic Acid Regenerated Mori, Tussah, Eri, Thai, and Muga Silk Materials: Mechanism of Self-Assembly. *ACS Biomater. Sci. Eng.* **2019**, *5*, 6361−6373.
(48) Saikia, A. K.; Goowalla, H. A Study on the Socio-Economic Condition of Women of Missing Community in Assam: An Overview. *J. Arts Soc. Sci.* **2016**, *1*, 10−13.
(49) Lai, S. K.; Wang, Y.-Y.; Wirtz, D.; Hanes, J. Micro- and Macrorheology of Mucus. *Adv. Drug Deliv. Rev.* **2009**, *61*, 86−100.
(50) Li, J.; Wan, H.; Ye, Y.; Zhou, H.; Chen, J. One-Step Process to Fabrication of Transparent Superhydrophobic SiO 2 Paper. *Appl. Surf. Sci.* **2012**, *261*, 470−472.
(51) Zhang, L.; Zhou, A. G.; Sun, B. R.; Chen, K. S.; Yu, H. Z. Functional and Versatile Superhydrophobic Coatings via Stoichiometric Silanization. *Nat. Commun.* **2021**, *12*, No. 982.
(52) Gogoi, P.; Chattopadhyay, A.; Pattader, P. S. G. Toward Controlling Evaporative Deposition: Effects of Substrate, Solvent, and Solute. *J. Phys. Chem. B* **2020**, *124*, 11530−11539.
(53) Saner, C. K.; Lusker, K. L.; LeJeune, Z. M.; Serem, W. K.; Garno, J. C. Self-Assembly of Octadecyltrichlorosilane: Surface

https://doi.org/10.1021/acsabm.1c00851
ACS Appl. Bio Mater. XXXX, XXX, XXX−XXX

Structures Formed Using Different Protocols of Particle Lithography. *Beilstein J. Nanotechnol.* **2012**, *3*, 114−122.
(54) Bhandaru, N.; Mukherjee, R. Ordering in Dewetting of a Thin Polymer Bilayer with a Topographically Patterned Interface. *Macromolecules* **2021**, *54*, 4517−4530.

https://doi.org/10.1021/acsabm.1c00851
ACS Appl. Bio Mater. XXXX, XXX, XXX−XXX